ATI 2015 - 70th Conference of the ATI Engineering Association

Evaluation of the radial flow effects on micro HAWTs through the use of a transition CFD 3D model - Part II: Post-processing and comparison of the results

Rosario Lanzafame[a], Stefano Mauro[a]*, Michele. Messina[a]

[a]Department of Industrial Engineering University of Catania, Viale A. Doria, 6 – 95125 Catania, Italy

Abstract

The importance and the complexity of the phenomena related to the development of radial flows is demonstrated in the first part of this paper. In order to further study the radial flow effects and to extend the analysis to laminar and transitional flows, the authors used a CFD 3D model, validated in the wind tunnel owned by the University of Catania. In the second part of this paper, the authors describe the strategy which was used to post-process the simulation results. Furthermore, a comparison of the results was made. Several simulations were first carried out at various wind and rotational speeds. Angles of Attack and aerodynamic coefficients were evaluated on cylindrical surfaces at different radial stations using the ANSYS Fluent Solver and ANSYS Post. Local velocities and forces, related to the sectional airfoil, were obtained in each cylindrical surface along with pressure coefficient distributions. In this way, it was possible to demonstrate the close relationship between radial flows and the strong depressurization of the suction side of the blade. Moreover, the results proved that the increase of lift and drag coefficients is linked to rotational speed and Angle of Attack as well. The radial effects were found to be enforced by laminar and transitional flows related to low Reynolds numbers. This will affect both design and analysis of wind rotor performance, more so than that which was originally suggested by empirical stall delay models.

*Keywords:*Horizontal Axis Wind Turbines; CFD; Transition Turbulence Modeling; 3D Radial Flows; Stall Delay Prediction

---

Nomenclature

C_p	Pressure Coefficient [-]		λ	Tip Speed Ratio [-]
α	Angle of Attack [deg]		C_l	Lift Coefficient [-]
V_1	Airfoil relative velocity [-]		C_d	Drag Coefficient [-]
ρ	Air density [kg/m^3]	r	Local radius [m]	
Re	Reynolds Number [-]		θ	Twist angle [deg]

---

* Corresponding author. Tel.: +39-095-7382414; fax: +39 095 337994
E-mail address: mstefano@diim.unict.it

c	Chord [m]		a	Axial induction factor [-]
ω	Angular speed [r/min]		V_0	Wind Speed [m/s]
ϕ	Incoming flow angle [deg]		R	Rotor Radius [m]
P_d	Local dynamic pressure [Pa]	F_d	Local dynamic force [N/m]

1. Post - processing strategy

Post processing the results of the 3D simulations and obtaining useful data for the evaluation of the radial effects is not a trivial problem. Concepts like angle of attack, aerodynamic coefficients and pressure coefficients are inherently 2D while the complex flow of a real rotating blade is strictly 3D.

Based on considerations from literature [1, 2], a procedure was implemented to extract sectional data of AoAs, lift and drag coefficients, pressure coefficients and flow-field images from 3D computations [7 - 9], using ANSYS CFD post.
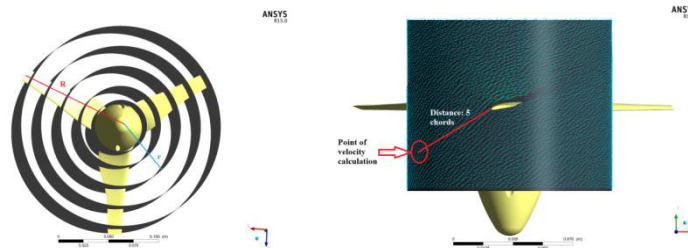

Fig. 1 Cylindrical surfaces for velocity post processing (left) and detail of the extrapolation technique (right)

First of all, five cylindrical surfaces were generated at different radial sections: r = 0.026 m (27% of radius R); r = 0.04 m (38% of radius R); r = 0.06 m (57% of radius R); r = 0.08 m (76% the radius R); r = 0.1 m (95% of radius R). Axial and tangential velocities were calculated on these surfaces using the ANSYS CFD turbo post. The velocities were calculated on a cylindrical surface at a distance of five chords in the mean flow direction, that is the relative flow direction seen by the airfoil in that cylindrical section. The images reported in Fig. 1, clarify the proposed methodology.

Knowing the axial (Va) and tangential (Vt) components of the relative velocity in a cylindrical section and the local twist angle θ [1, 2] it was possible to determine the local AoA α as presented in Fig. 2. Here V1 is the local relative velocity, V0(1-a) is equal to the calculated axial component Va and ωr(1+a') is equal to the tangential component Vt , with a and a' as the axial and tangential induction factors.

As the local flow angle ϕ is defined as:

$$\phi = \arctan\left(\frac{(1-a)V_0}{(1+a')\omega r}\right) = \arctan\left(\frac{V_a}{V_t}\right) \tag{1}$$

From Fig. 2 the calculated AoA is:

$$\alpha = \phi - \theta \tag{2}$$

The induction factors were not necessary as the real velocity were obtained post processing the CFD results.

Comparing this methodology to that of Johansen and Sørensen [1, 2] similar results were obtained.

Once extracted the AoAs, the force distribution in x (Fx) and y (Fy) direction (Fig. 2) were calculated in every cylindrical section, on the sectional aerofoil, using the "forcenorm" CFD post tool. Referring to the notation of Fig. 2 the lift and drag forces can be determined as follows:
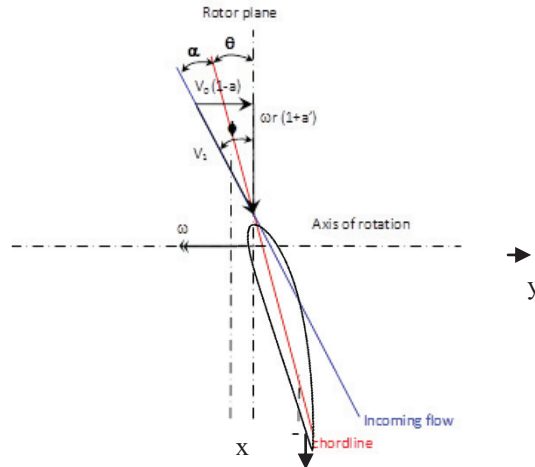
Fig. 2 Velocity components on a local section

$$L = F_y \cos\phi - F_x \sin\phi \tag{3}$$

$$D = F_y \sin\phi + F_x \cos\phi \tag{4}$$

The non-dimensional lift and drag coefficients are hence obtained calculating the local dynamic pressure in the considered cylindrical section (5), dividing L (3) and D (4) for the local dynamic force Fd (6).

$$p_d = \frac{1}{2}\rho V_1^2 \tag{5}$$

$$F_d = p_d c \tag{6}$$

Where ρ = 1.225 kg/m3; V1 is the local relative velocity calculated from Va and Vt; c is the local chord, variable along the radius as the blade was tapered.

Furthermore, the local dynamic pressure (5) was used for calculating the distribution of the pressure coefficient, Cp (7), in each airfoil section. This non-dimensionalization allowed for an adequate comparison of the pressure distribution at the different radial sections and at the different operative conditions. In this way, the effects of radial flow on the pressure distribution over the sectional airfoil could be correctly evaluated.

$$C_p = \frac{p - p_\infty}{p_d} \tag{7}$$

Where p is the calculated pressure over the sectional airfoil, p∞ is the reference pressure at the inlet of the domain and pd is the aforementioned local dynamic pressure (5). In this way the spanwise pressure gradient can be decoupled and only the centrifugal and Coriolis effects influence the Cp distribution and hence Cl and Cd.

2. Comparison of the results

All simulations were post processed in order to extract the 3D AoAs, lift and drag coefficients. Obviously the Reynolds number is quite variable therefore it does not make sense to refer the data to a

specific Re. However the range of variation of the Reynolds numbers was found to be between 7,000 and 76,000, where laminar and transitional effects are considerable.

In the charts below (Fig. 3, 4, 5), lift and drag coefficients are presented as a function of AoA at different radial stations. The pure 2D CFD data [7, 8, 9] are reported along with Cl experimental data for a Reynolds number of 106 [10] in order to highlight the 3D and low Re effects, even because these experimental data were used in the 1D BEM code for the design of the rotor. Fixing the wind speed, the lower AoAs correspond to the higher rotational speed, as indicated in the charts. In order to be concise only 5, 15 and 30 m/s data are presented. The AoA of maximum peak of Cl is displayed as well.

As can be seen from Figures 3, 4 and 5, the lift coefficient augmentation, experienced by other othors was confirmed here. Specifically, in the range between 10° and 60° of AoA, the comparison with pure 2D CFD data showed a great increase of the lift forces due to centrifugal effects [3 - 6]. The peak was found around 35° where the combination of radial flow and stall conditions generated a non-dimensional force which was twice the 2D force. This indicates a general increment of the resultant of the aerodynamic forces due to rotation in all the range of separated flows. The inner part of the blade was confirmed to be more influenced by the centrifugal effects [3 - 6], above all at r/R = 38%, where the hub effects were not so important. However, the increment of the forces was found to be related to a particular combination of stall, rotational speed and AoA. For example, also at r/R = 57%, in Fig. 3 and Fig. 4, the lift and drag coefficients are higher than the other values. As expected, instead, at the tip (r/R = 95%) the forces were lower due to tip losses [3 - 6].

The effects of the radial flow therefore influence lift and drag, depending on the geometrical AoA and rotational speed. In fact, at lower AoAs (10° < α < 40°), the resultant of the forces gave the maximum effects on the lift forces while at higher AoAs (α > 40°) the lift augmentation was gradually reduced, increasing the drag coefficient. At α > 60°, the force augmentation was found to be of minor importance because of the lower rotational speed and higher AoAs. In this case, the aerodynamic coefficients were found to be comparable to pure 2D data. At α < 10°, instead, the flow seemed to be attached and the radial effects were drastically reduced as reported in the literature [3 - 6]. Calculated 3D Cl and Cd in fact matched the 2D CFD data.

In order to underline the laminar and transitional effects, the difference with 2D Cl experimental data was also highlighted as related to a higher Reynolds number (1 million) [10]. At lower AoA (α < 15°) the turbulent behavior generates higher lift coefficients, the flow remains attached and higher forces are generated. In the same range, at lower Reynolds numbers, both 2D and 3D sectional data were heavily influenced by laminar effects like separation bubbles that drastically reduce the lift forces. For α > 15° the radial effects generate a centrifugal vortex along the blade (Fig. 6), depressurizing the boundary layer and drastically increasing the lift forces, well above the values for Re = 1 million. This emphasizes the importance of the use of proper aerodynamic coefficient data in the 1D BEM modeling and to take in more significant account the radial effects. This is important above all at lower Reynolds numbers, where the combination of laminar and centrifugal effects completely distort the aerodynamic behavior if compared to the simple 2D conditions.

Furthermore, comparing 2D and 3D sectional results, a different orientation of the resultant R of the forces was found. This leads to a further increment of the lift coefficients and this is likely due to the change in the pressure distribution over the 3D sectional airfoil, generated by rotation.

Essentially, it was found that the radial flow acts on the blade depressurizing the suction side, increasing the resultant of the aerodynamic forces R and deflecting it towards the leading edge. The laminar and transitional effects further increase the radial flow development as, at low Reynolds numbers, the flow-field is quite unstable and sensitive to separation. The radial flow depends on separation, in turn, so the final effect was found to be an unexpected great increase of the rotor performance, generated by centrifugal effects when operating in fully stalled conditions
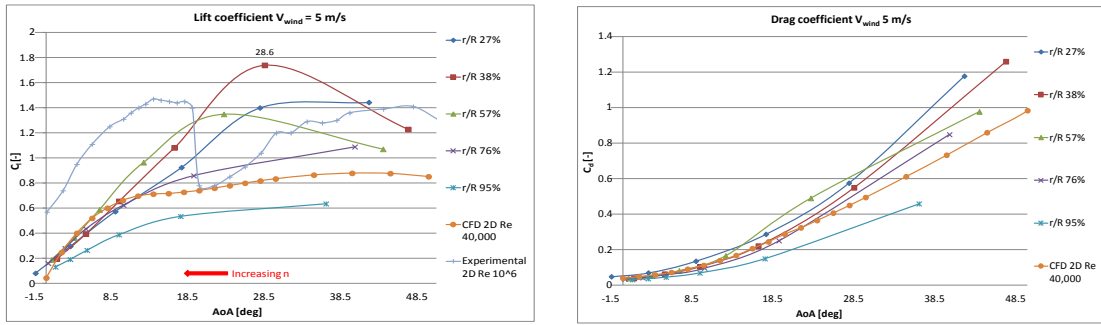
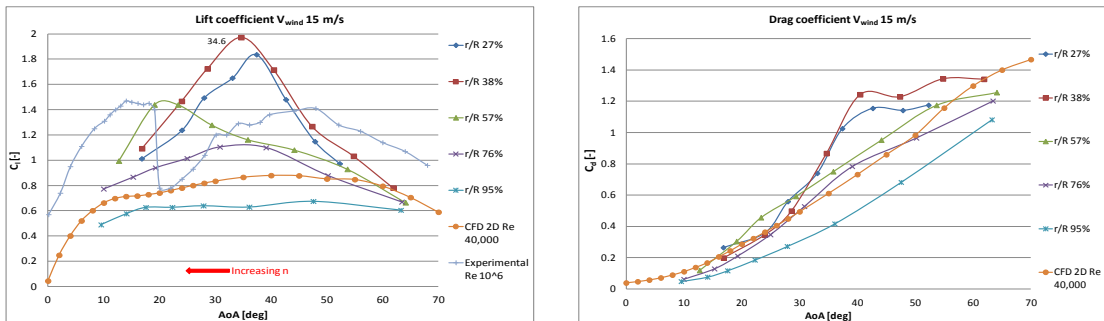Fig. 3 Lift (lef) and drag (right) coefficients for wind speed 5 m/s (7,000 < Re < 12,200)

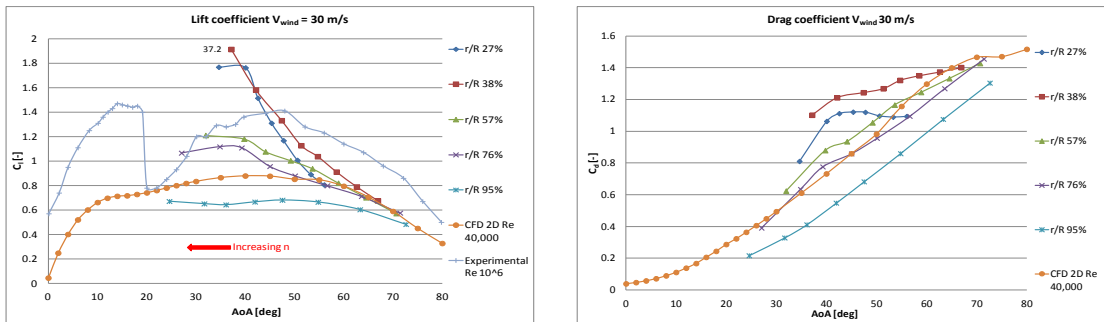Fig. 4 Lift (left) and drag (right) coefficients for wind speed 15 m/s (15,100 < Re < 48,700)

Fig. 5 Lift (left) and drag (right) coefficients for wind speed 30 m/s (28,800 < Re < 76,300)

The above is supported by the following analyses and comparison, proposed in Tab. I. Here, three different AoAs were compared, extrapolating sectional 3D data and pure 2D CFD results. The flow-field was related to the trend of the pressure coefficient in order to evaluate the change in pressure distribution over the sectional airfoil. The 3D data were calculated in the inner section of the blade (r/R 38%) where the maximum effect of radial flow was experienced.

At $\alpha \approx 10°$ (Tab. I a and b) the pure 2D flow-field presents a slight separation due to the laminar instability while in the 3D condition, the flow seems to be attached. The lift and drag coefficients are comparable. The pressure coefficient distribution is similar and this explains the substantial equality of the aerodynamic coefficients. This means that the centrifugal effects, in this case, thin the boundary layer and reduce the laminar bubble effects, detectable in the oscillation of the trend of the Cp in the suction

side of the 2D case (Tab. I a). However, no further depressurization was generated, because the deviation of the fluid particle was limited by the reattachment.

The behavior at $\alpha \approx 35°$ was significant (Tab. I c and d). Here, the maximum lift augmentation was found and the explanation is clear looking at both flow-field vectors and pressure coefficient distribution.

The recirculation area in the suction side of the profile thinned drastically due to the development of the radial flow. The differences with 2D results are considerable, as the flow appeared to be nearly reattached. The great depressurization generated by rotation is evidenced when comparing 2D and 3D pressure coefficient charts. The suction side of the 3D case (d) has a minimum Cp of -6.5 near the leading edge and a mean value under -1.5 in a vast portion of the suction side while the 2D case presents a typical pressure distribution of a stalled condition, with a mean Cp higher than -0.6. This is explains why, in this condition, the 3D lift coefficient is more than twice the 2D lift coefficient. In this range of medium AoAs and higher rotational speeds, the combination of separation and radial flow generates the maximum depressurization and hence the higher forces compared to simple 2D conditions.

At higher AoAs, $\alpha \approx 60°$ (Tab. I e and f), the differences in the flow-field are quite limited because lower rotational speed does not allow the stall to be overcome. Only a slight increase in both lift and drag coefficients can be found and this is confirmed looking at the Cp comparison. The minimum peak of Cp is -2.3 near the leading edge, while 2D Cp is -1.2, but the stall conditions generate the same trend in a great portion of the suction side, with comparable values of Cp.

It was found, in general, that the increase of the aerodynamic forces, generated by centrifugal flows, regards the entire blade up to r/R 76%, with higher values in the inner sections. Thus also occurs when the combination of high rotational speeds and stall conditions lead to a considerable depressurization of the suction side. The laminar flow conditions, related to the present work, enforces the centrifugal pumping effects in a wide range of AoAs, considerably more than what was seen in the literature. However, no stall delay was detected because no separation point was found, as the laminar conditions always led to a leading edge stall.

In Fig. 6, a comparison between the streamlines on the pressure side and on the suction side of the blade is presented. The development of a deep radial flow on the suction side is highlighted (wind speed 15 m/s; rotational speed 2,500 r/min). On the pressure side, instead, the flow is well guided and not deflected so the radial flow is not present.
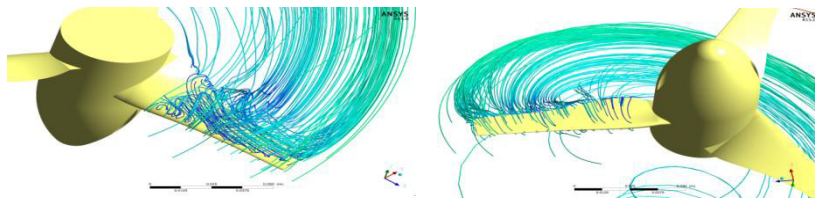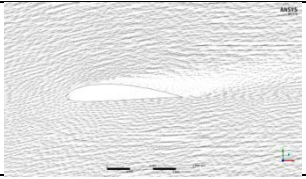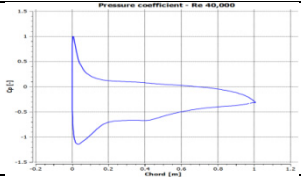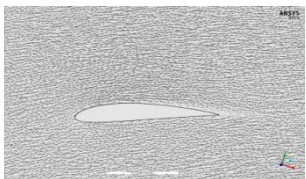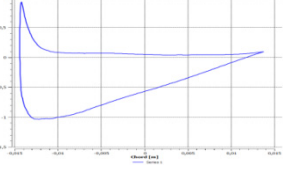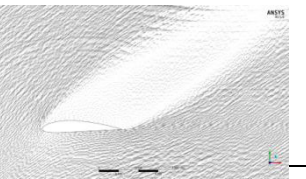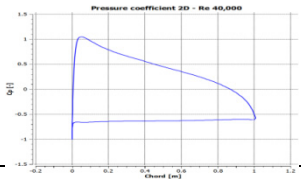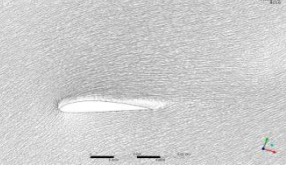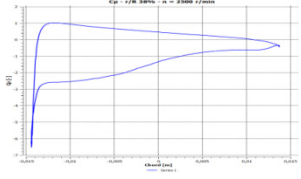

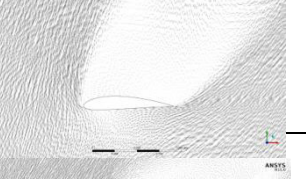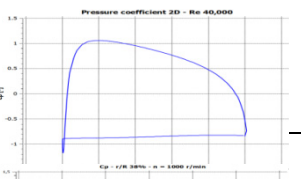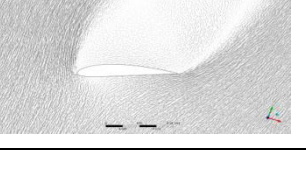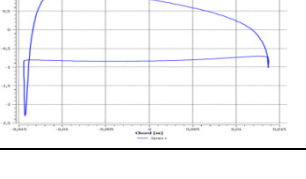Fig. 6 Streamlines of velocity for suction side (left) and pressure side (right). (V_0 = 15 m/s; n = 2,500 r/min)

3. Conclusions

After reviewing the scientific literature and the numerical CFD model, which was implemented by the authors in the first part of this paper, the effects of the radial flow on a micro HAWT were able to be extensively evaluated, thus making post processing the CFD 3D results possible.

Table. 1. Sectional airfoil data comparison

	Data	Vectors of flow-field	Coefficient of pressure
a	CFD 2D Re = 40,000 AoA = 10° C_l = 0.662 C_d = 0.111 Minimum C_p = -1.15		
b	CFD 3D Re = 19,900 AoA = 9.5° C_l = 0.656 C_d = 0.104 V_0 = 5 m/s n = 2,000 r/min Minimum C_p = -1.02		
c	CFD 2D Re = 40,000 AoA = 35° C_l = 0.865 C_d = 0.611 Minimum C_p = -1		
d	CFD 3D Re = 36,500 AoA = 34.6° C_l = 1.97 C_d = 0.867 V_0 = 15 m/s n = 2,500 r/min Minimum C_p = -6.5		
e	CFD 2D Re = 40,000 AoA = 60° C_l = 0.795 C_d = 1.298 Minimum C_p = -1.2		
f	CFD 3D Re = 48,400 AoA = 60.1° C_l = 0.83 C_d = 1.36 V_0 = 25 m/s n = 1,000 r/min Minimum C_p = -2.3		

The CFD model, based on a calibrated transition turbulence model, was developed and validated using a prototype, designed and tested in the sub-sonic wind tunnel owned by the University of Catania.

In the validation range of the model, a procedure to extract sectional airfoil data at different radial stations is presented. Specifically, 3D angles of attack, lift, drag and pressure coefficients were extrapolated on five concentric cylindrical surfaces, in a wide range of operating conditions. The results were compared to pure 2D CFD results in order to accurately evaluate the stall delay and aerodynamic force augmentations, mentioned in the reviewed literature. Furthermore, the combined effects of radial

and laminar flows in a rotating blade were able to be further evaluated, demonstrating results of significant interest.

In particular, the aerodynamic forces augmentation, generated by rotation, was confirmed in a wide range of AoAs (from 10° to 60°), as both lift and drag coefficients were considerably increased, above all around 30° - 40°. In this range of AoAs, the combination of high rotational velocity and stall conditions cause a substantial depressurization of the suction side of the airfoil. This was evaluated comparing vector fields and pressure coefficients of 2D and 3D simulations. The resultant of the aerodynamic forces was thus increased. Moreover, a different orientation of the resultant towards the leading edge, was detected. This change in the orientation was due to the differences in pressure distribution, thus influencing the aerodynamic coefficients as well.

In conclusion, it was found that low Reynolds numbers strengthen the phenomenon of the radial flow as the laminar sensitivity to separation leads to an increase and extension of the centrifugal pumping. This suggests that the traditional post-stall model may not be suitable at low Re.

A close link between rotational speed and depressurization of the suction side of the blade was detected as well, suggesting a predominant tie to centrifugal force. This will be further examined in future research.

References

[1] Jeppe Johansen, Niels N. Sørensen Aerofoil Characteristics from 3D CFD Rotor Computations Wind Energy 2004; **7**:283–294 (DOI: 10.1002/we.127)

[2] Wen Z. Shen, Martin O. L. Hansen and J. N. Sørensen, Determination of the Angle of Attack on Rotor Blades Wind Energy 2009; 12:91–98, (DOI: 10.1002/we.277)

[3] Carlo E. Carcangiu, Jens N. Sørensen, Francesco Cambuli, Natalino MandasCFD–RANS analysis of the rotational effects on theboundary layer of wind turbine bladesJournal of Physics: Conference Series 75 (2007) 012031 doi:10.1088/1742-6596/75/1/012031

[4] Guohua Yu, Xin Shen, Xiaocheng Zhu, Zhaohui DuAn insight into the separate flow and stall delay for HAWTRenewable Energy 36 (2011) 69 - 76

[5] S. Hauptmann, S. Streiner, F. Kunert, M. Kühn, P. Dörr, P. W. ChengConsideration of the Aerodynamic Effects of Blade Rotation as Computed with URANS in Load Simulations with BEM. EWEA Proceedings 2012

[6] Iván Herráez, Bernhard Stoevesandt**,** Joachim Peinke Insight into Rotational Effects on aWind Turbine Blade UsingNavier–Stokes ComputationsEnergies 2014, 7, 6798-6822; doi:10.3390/en7106798

[7] Lanzafame R., Mauro S., Messina M. Wind turbine CFD modeling using a correlation-basedtransitional model Renewable Energy 52 (2013) 31 - 39 - Elsevier

[8] R. B. Langtry, F. R. Menter, S. R. Likki, Y. B. Suzen, P. G. Huang and S. Völker, 2006, "ACorrelation-Based Transition Model Using Local Variables—Part I: Model Formulation" Vienna, 498 ASME Paper No. ASME-GT2004-53452. 499

[9] R. B. Langtry, F. R. Menter, S. R. Likki, Y. B. Suzen, P. G. Huang and S. Völker, 2006, "ACorrelation-Based Transition Model Using Local Variables—Part II: Test Cases and Industrial 501 Applications" ASME J. Turbomachinery, 128 (3), pp. 423–434

[10] R. L. Reuss, M. J. Hoffmann, G. M. Gregorek Effects of Surface Roughness and Vortex Generators on the NACA 4415 Airfoil - The Ohio State University, Columbus, Ohio, December 1995 NREL/TP-442-6472
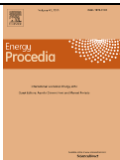
Biography

Stefano Mauro is a Research Fellow at University of Catania. He has a PhD in "Energetic System and Environment". His research mainly deal with CFD, Aerodynamics, Turbulence Modeling, Wind Turbines, Internal Combustion Engine and Fluid Machinery in general. He published 2 works on international journal regarding Wind Turbines CFD modeling.